Bioenergetics and mitochondrial transmembrane potential during differentiation of cultured osteoblasts

Svetlana V. Komarova, Fasoil I. Ataullakhanov and Ruth K. Globus

Am J Physiol Cell Physiol 279:1220-1229, 2000.

Am J Physiol Cell Physiol
279: C1220–C1229, 2000.

Bioenergetics and mitochondrial transmembrane potential during differentiation of cultured osteoblasts

SVETLANA V. KOMAROVA,[1] FASOIL I. ATAULLAKHANOV,[2] AND RUTH K. GLOBUS[1]
[1]*Life Sciences Division, NASA Ames Research Center, Moffett Field, California 94035-1000; and* [1]*National Research Center for Hematology, Moscow, 125167 Russia*

Received 13 January 2000; accepted in final form 2 May 2000

Komarova, Svetlana V., Fasoil I. Ataullakhanov, and Ruth K. Globus. Bioenergetics and mitochondrial transmembrane potential during differentiation of cultured osteoblasts. *Am J Physiol Cell Physiol* 279: C1220–C1229, 2000.—To evaluate the relationship between osteoblast differentiation and bioenergetics, cultured primary osteoblasts from fetal rat calvaria were grown in medium supplemented with ascorbate to induce differentiation. Before ascorbate treatment, the rate of glucose consumption was 320 $nmol \cdot h^{-1} \cdot 10^6$ $cells^{-1}$, respiration was 40 $nmol \cdot h^{-1} \cdot 10^6$ $cells^{-1}$, and the ratio of lactate production to glucose consumption was ~2, indicating that glycolysis was the main energy source for immature osteoblasts. Ascorbate treatment for 14 days led to a fourfold increase in respiration, a threefold increase in ATP production, and a fivefold increase in ATP content compared with that shown in immature cells. Confocal imaging of mitochondria stained with a transmembrane potential-sensitive vital dye showed that mature cells possessed abundant amounts of high-transmembrane-potential mitochondria, which were concentrated near the culture medium-facing surface. Acute treatment of mature osteoblasts with metabolic inhibitors showed that the rate of glycolysis rose to maintain the cellular energy supply constant. Thus progressive differentiation coincided with changes in cellular metabolism and mitochondrial activity, which are likely to play key roles in osteoblast function.

ATP; respiration; glycolysis; bone

ROBUST DEMANDS FOR ENERGY are placed on osteoblasts during production of a mineralized matrix, which provides both structural support and a calcium reservoir. Although oxidative phosphorylation produces 17 times more ATP per mole of glucose than glycolysis, both pathways participate in the response of bone cells to calciotropic stimuli (31). Treatment of young rats with parathyroid hormone (PTH) increases glycolytic activity of bone tissue (4). Furthermore, gonadal steroids stimulate the enzymatic activity of creatine kinase, which transfers phosphate from creatine to generate ATP (32). Mechanical loading affects blood flow in bone and, consequently, oxygenation; conversely, skeletal disuse induces hypoxia in osteocytes (8). Thus the activities of bioenergetic pathways in osteoblasts are likely to play key roles in the physiology of skeletal tissue.

Mitochondria are diverse in both form and function, and they participate in various critical cell functions in addition to bioenergetics, including apoptosis and calcium signaling (12, 15). Oxidative ATP synthesis is driven by an electrochemical gradient across the inner mitochondrial membrane, which comprises differences in both pH and transmembrane potential ($\Delta\psi$). There is a direct correlation between the energized state of mitochondria and the $\Delta\psi$ when analyzed in isolated mitochondria (28). Recent studies that used the fluorescent vital dye 5,5′,6,6′-tetrachloro-1,1′,3,3′-tetraethylbenzimidazolcarbocyanine iodine (JC-1), which preferentially accumulates in mitochondria by a $\Delta\psi$-dependent mechanism, revealed that individual mitochondria undergo large changes in $\Delta\psi$ and in subcellular distribution in response to a variety of stimuli, including apoptosis, receptor activation, and hypoxia (5).

Remarkably little is known about how mitochondrial activity and the principal pathways of energy metabolism are regulated during osteoblast differentiation. Previous studies on energy metabolism used bone slices or bone marrow stromal cultures, which contain multiple cell types, or cultures of bone cells, which are not yet fully mature (4, 9, 20, 21, 30). However, the techniques of primary bone cell culture have advanced sufficiently to assess biochemical and molecular changes in osteoblasts at various well-defined stages of differentiation once isolated from the complexities of intact bone. In primary cultures of bone cells, treatment with ascorbic acid (AA) and β-glycerophosphate (βGP) leads to production of a mineralized matrix and expression of a phenotype characteristic of mature osteoblasts. This process entails a progressive sequence of morphogenic events, including proliferation and multilayering, synthesis of an abundant extracellular matrix, mineralization of that matrix, and, finally, differentiation into osteocyte-like cells or apoptosis (11, 23, 24, 26, 27).

The aim of this study was to identify changes in bioenergetic pathways (glycolysis, oxidative phosphor-

Address for reprint requests and other correspondence: R. K. Globus, MS 236–7, Life Sciences Division, NASA Ames Research Center, Moffett Field, CA 94035-1000 (E-mail: rglobus@mail.arc.nasa.gov).

The costs of publication of this article were defrayed in part by the payment of page charges. The article must therefore be hereby marked "*advertisement*" in accordance with 18 U.S.C. Section 1734 solely to indicate this fact.

ylation) and mitochondrial activity ($\Delta\psi$) that occur at different stages of osteoblast differentiation and then to evaluate the contribution of these pathways to the maintenance of the ATP content of mature osteoblasts at steady state. We found that cellular bioenergetics and $\Delta\psi$ were differentially regulated during differentiation, perhaps functioning to maintain the relatively high ATP content observed in mature osteoblasts compared with immature cells.

MATERIALS AND METHODS

Cell culture. Cells were isolated from 21-day-old fetal rat calvaria as previously described (26). All animal procedures were reviewed and approved by the Institutional Animal Care and Use Committee at NASA Ames Research Center. Briefly, cells were plated at a density of 36,000 cells/cm^2 on eight-well chamber slides (0.81 cm^2 per well; Permanox, Nunc, Naperville, IL) coated with 0.2% gelatin (Sigma, St. Louis, MO) and then cross-linked with carbodiimide. Cells were grown in α-MEM (GIBCO, Grand Island, NY) supplemented with 10% serum (GIBCO) in 5% CO_2 at 37°C for the indicated times. After the cultures achieved confluence (*day 3*), cells were induced to differentiate by the addition to the culture medium of freshly prepared AA (50 μg/ml), which is needed for matrix formation, and βGP (3 mM), which is needed for mineralization. To maintain cells in an immature state, cultures were grown continuously without these additives. The media were changed every 2–3 days. Samples were recovered on *day 3* (before the addition of AA and βGP) or at the indicated times after growth in the presence or absence of AA and βGP and then were stored at −20°C until later analysis.

Cell number. Cultures were treated sequentially with PBS, pH 7.4, containing 10 mM EGTA and 20 mM HEPES, pH 7.4, for 20 min and then for 60 min at 37°C with 572 U/ml collagenase in 115 mM NaCl, 5.3 mM KCl, 3 mM K_2HPO_4, 1 mM $CaCl_2$, 30 mM mannitol, 10 mM glucose, 2 g/l BSA, and 24 mM HEPES, pH 7.4. An equal volume of 0.25% trypsin in EDTA (1 mM) in Hanks' balanced salt solution without Ca^{2+} and Mg^{2+} (GIBCO) was added to the collagenase, and cells were incubated for another 30 min. Dispersed cells were counted using a hemocytometer. Exclusion of 0.1% trypan blue in saline was used to determine cell viability, which was typically 80–90% of the total cell population.

Glucose consumption and lactate production. Concentrations of glucose and lactate in media were measured using a model 2700 select analyzer from Yellow Springs Instruments (Yellow Springs, OH). The rates of glucose consumption ($\dot{V}_{glu}$) and lactate production ($\dot{V}_{lac}$) were shown to be linear over 6 h of incubation (data not shown). Medium samples (0.05 ml) were recovered between 2 and 6 h of incubation with cells. $\dot{V}_{glu}$ or $\dot{V}_{lac}$ were calculated as the difference between initial and final concentration divided by incubation time.

O_2 consumption and ATP production. O_2 consumption ($\dot{V}O_2$) was measured in culture medium at 37°C with a polarographic O_2 electrode (Radiometer, Copenhagen, Denmark) installed into one well of an eight-well chamber slide to form an air-tight seal. At the indicated times in culture, the concentration of O_2 was measured in medium containing HEPES (10 mM), and $\dot{V}O_2$ was determined over 60 min. $\dot{V}O_2$ decreased to zero when cells were treated with sodium azide (NaN_3) or potassium cyanide (KCN), showing that changes in $\dot{V}O_2$ measured in culture medium were due to mitochondrial respiration. The addition of HEPES did not affect the rates of $\dot{V}_{glu}$ and $\dot{V}_{lac}$ or ATP concentration in osteoblasts during 4 h of incubation (data not shown). Total ATP production from glucose in mature osteoblasts was estimated on the basis of the assumption that anaerobic glycolysis produces 2 mol of ATP from 1 mol of glucose and reduction of 1 mol of O_2 is coupled to the production of 6 mol of ATP.

Alkaline phosphatase and ATP content. To measure alkaline phosphatase activity and ATP, cultures were extracted in 1% Triton X-100 in HEPES buffer, pH 7.4, and then sonicated and centrifuged at 10,000 *g* for 3 min. Supernatants were stored at −80°C until analysis. Alkaline phosphatase activity and ATP content were measured spectrophotometrically (Spectronic 1001 plus, Milton Roy) with commercial kits (Sigma). The alkaline phosphatase assay measured the hydrolysis of *p*-nitrophenol phosphate, and the ATP assay used the phosphoglycerate phosphokinase and phosphate dehydrogenase reactions, which couple the utilization of ATP with the oxidation of NADH to NAD.

Flow cytometry. Flow cytometry was used to estimate cell size in mature and immature populations of osteoblasts. Cells were dispersed as described in *Cell number* and then prepared for cytometric analysis as described in detail by Ilic et al. (16). The viable and apoptotic cell populations were distinguished according to a cytometric method (14). In brief, dispersed cells were incubated with propidium iodide (PI; 5 μg/ml) on ice for 15 min before the addition of Hoechst 33342 dye (Molecular Probes, Eugene, OR). After a further 6-min incubation at room temperature, samples were acquired with the use of a dual-laser FACStar cell sorter (Becton-Dickinson, San Jose, CA) until 20,000 cells were analyzed. Cells that stained weakly for PI and Hoechst dye (viable cells) comprised 75–85% of the total cell population recovered. Cell size was assessed by forward light scatter. The flow cytometry data shown are representative of two separate experiments.

Staining and confocal microscopy. Mineralized nodules in mature cultures (*day 14*) were demonstrated by alizarin red S staining of calcium salts. Cells were fixed in ethanol, stained for 60 min in 1% alizarin red S in distilled water, pH 6.4, and then washed with distilled water. Images of osteoblasts at different stages of differentiation were acquired at the indicated times using an inverted scanning confocal microscope (Zeiss LSM 510) equipped with differential interference contrast optics.

Mitochondrial $\Delta\psi$ was assessed in live cells with the use of the fluorescent probe JC-1 (25, 29, 33). JC-1 accumulates in mitochondria as a function of $\Delta\psi$, is excited at 490 nm, and emits at 527 nm when in monomeric form. At high $\Delta\psi$, JC-1 is concentrated within mitochondria and forms J aggregates, resulting in a shift in emission to 585 nm. Cells grown in eight-well chamber slides (Permanox, Nunc) were incubated with JC-1 (10 μg/ml) in fresh culture medium for 30 min at 37°C and 5% CO_2 before analysis. In addition, cells were grown on glass coverslips so that image stacks could be collected in the reverse sequence (bottom of nodule to top, rather than top of nodule to bottom). After incubation with JC-1, the cells were washed three times with culture medium, and a glass coverslip was placed over the cells, which were immersed in fresh medium.

Images were collected using a Zeiss LSM 510 microscope equipped with a 30-mW argon-krypton laser and a ×100 objective with numerical aperture of 1.3. Low-$\Delta\psi$ mitochondria (green) were observed with a 505- to 550-nm band-pass emission filter under 488-nm laser illumination. High-$\Delta\psi$ mitochondria (red) were observed with a 585-nm long-pass emission filter under 568-nm laser illumination. Pin hole sizes and photomultipliers were set to produce the clearest

possible image without saturating the signal. After conditions of image acquisition for differentiated cells in nodules were optimized, images of immature cells were collected using identical settings. The data shown are representative of at least three different fields in three separate experiments. To provide a quantitative estimate of the differences in fluorescence between images, the total number of pixels in the red channel was divided by the total number of pixels in the green channel for each image.

Metabolic inhibitors. Cells were grown in medium containing AA and βGP for 14 days; the medium was then supplemented with sodium fluoride (NaF) (5–30 mM), NaN_3 (1–8 mM), or KCN (2–4 mM) for a 1-h preincubation period. Fresh medium was added with the addition of inhibitor, and changes in O_2 were measured for 2–4 h. Samples were recovered from cultures treated in parallel to measure glucose and lactate. ATP was measured after 4 h of incubation with inhibitor.

Statistics. The data shown are representative of four to six separate experiments performed in duplicate, and values are expressed as means ± SE. Statistical evaluation was made with ANOVA, using the software SuperANOVA (Abacus Concepts, Berkeley, CA).

RESULTS

Temporal sequence of osteoblast differentiation. Experimental protocols for the differentiation of primary osteoblasts typically entail growth for 3–4 wk of culture before nodule formation and mineralization (24, 27), whereas our protocol (see MATERIALS AND METHODS) results in a more rapid differentiation (26). Because both proliferation and maturation can influence cellular bioenergetic pathways, we therefore first carefully defined the temporal sequence of changes in cell number and differentiation, as assessed by nodule formation and alkaline phosphatase activity.

Osteoblasts were plated to achieve confluence by *day 3* in culture (Fig. 1*A*), at which time AA (50 μg/ml) and βGP (3 mM) were first added to the medium to induce differentiation. Cultures treated with AA and βGP have been referred to subsequently as AA-treated cells for simplicity. Paired cultures grown in medium without the addition of AA and βGP have been referred to as AA-untreated cells. Confluent cultures on *day 3* appeared morphologically flat and well spread (Fig. 1*A*). Treatment with AA resulted in the appearance of clusters of plump, cuboidal cells by *day 7* (Fig. 1*B*), a morphology characteristic of mature osteoblasts in vivo. The nodules became increasingly optically dense between *day 7* and *day 14* in culture (Fig. 1, *C* and *D*). Staining cultures with alizarin red to reveal mineralized matrix showed that, on *day 14*, AA-untreated cells were morphologically flat and the cell layers did not stain positively for calcified matrix (Fig. 1*E*), whereas nodules in AA-treated cell layers stained strongly for calcified matrix (Fig. 1*F*).

Cells continued to proliferate between *day 3* and *day 7* (postconfluence), forming multilayers (Fig. 2*A*). The rate of growth stabilized between *day 7* and *day 14* in AA-treated cultures, achieving a final cell density twofold higher than that in AA-untreated cultures (Fig. 2*A*). Thus growth of cells for various times in either AA-treated or AA-untreated medium provides the opportunity to distinguish between influences of cellular aging as opposed to differentiation.

Alkaline phosphatase activity was measured as an early marker of osteoblast differentiation (1–3). AA treatment caused a progressive rise in alkaline phosphatase activity to levels sevenfold higher on *day 14* than in cells grown without AA (Fig. 2*B*). In contrast, the alkaline phosphatase activity of cells grown without the addition of AA did not markedly change over time.

To summarize, cells treated with AA to induce differentiation continued to divide after confluence was achieved, forming multilayers within the first 7 days of culture when morphological evidence of nodule formation first appeared. Alkaline phosphatase activity progressively rose from *day 3* to *day 14* and plateaued thereafter, whereas morphogenesis and mineralization of nodules occurred between *day 7* and *day 14*.

Glycolytic and oxidative pathways. We measured $\dot{V}_{glu}$, $\dot{V}_{lac}$, and $\dot{V}O_2$ to assess glycolytic and oxidative components of energy metabolism at various times in culture (Fig. 3). $\dot{V}_{glu}$ in AA-untreated cultures decreased from 320 $nmol \cdot h^{-1} \cdot 10^6$ $cells^{-1}$ on *day 3* to 240 $nmol \cdot h^{-1} \cdot 10^6$ $cells^{-1}$ on *day 7* and remained at this level until the end of the experiment (*day 14*). AA treatment caused a transient decrease in $\dot{V}_{glu}$ (*days 3–7*) and subsequent increase to levels twofold higher than shown in AA-untreated cultures on *day 14* (Fig. 3*A*). In contrast, $\dot{V}_{lac}$ transiently decreased (*days 3–7*) in both AA-treated and AA-untreated cells (Fig. 3*B*) and was 2-fold lower on *day 7* and 1.4-fold higher on *day 14* in AA-treated compared with that in AA-untreated cells.

The temporal changes in $\dot{V}_{glu}$ and $\dot{V}_{lac}$ resulted in a transient twofold decrease in the ratio of $\dot{V}_{lac}$ to $\dot{V}_{glu}$ in AA-treated compared with AA-untreated cells on *days 7* and *10* (Fig. 3*C*). Changes in the ratio of $\dot{V}_{lac}$ to $\dot{V}_{glu}$ indicate that less of the pyruvate produced by glycolysis is converted to lactate, and thus these results are consistent with the possibility that respiration was higher in AA-treated cells on *days 7* and *10* than in AA-untreated cells. In fact, $\dot{V}O_2$ in AA-treated cells rose markedly (3-fold) from *day 3* to *day 7* and then remained elevated (Fig. 3*D*). In contrast, $\dot{V}O_2$ in AA-untreated cells did not change significantly over time. Together, these data show that respiration increased during the stage of cell multilayering and early nodule morphogenesis (*days 3–7*) and that both cell aging in culture and maturation contribute to the changes in glycolysis observed over time.

Mitochondrial transmembrane potential. We assessed the influence of differentiation on mitochondrial $\Delta\psi$ in live cells by confocal microscopy using the fluorescent dye JC-1. When stained with JC-1, mitochondria with $\Delta\psi$ below ~120 mV emit light in green wavelengths, whereas those with high $\Delta\psi$ emit light in red wavelengths (see MATERIALS AND METHODS). Figure 4 shows images captured from AA-untreated cultures and nodules of AA-treated cultures on *day 10* in culture (Fig. 4, *A–F*). Images collected from the most central regions of nodules, which consist of dense, mineralized

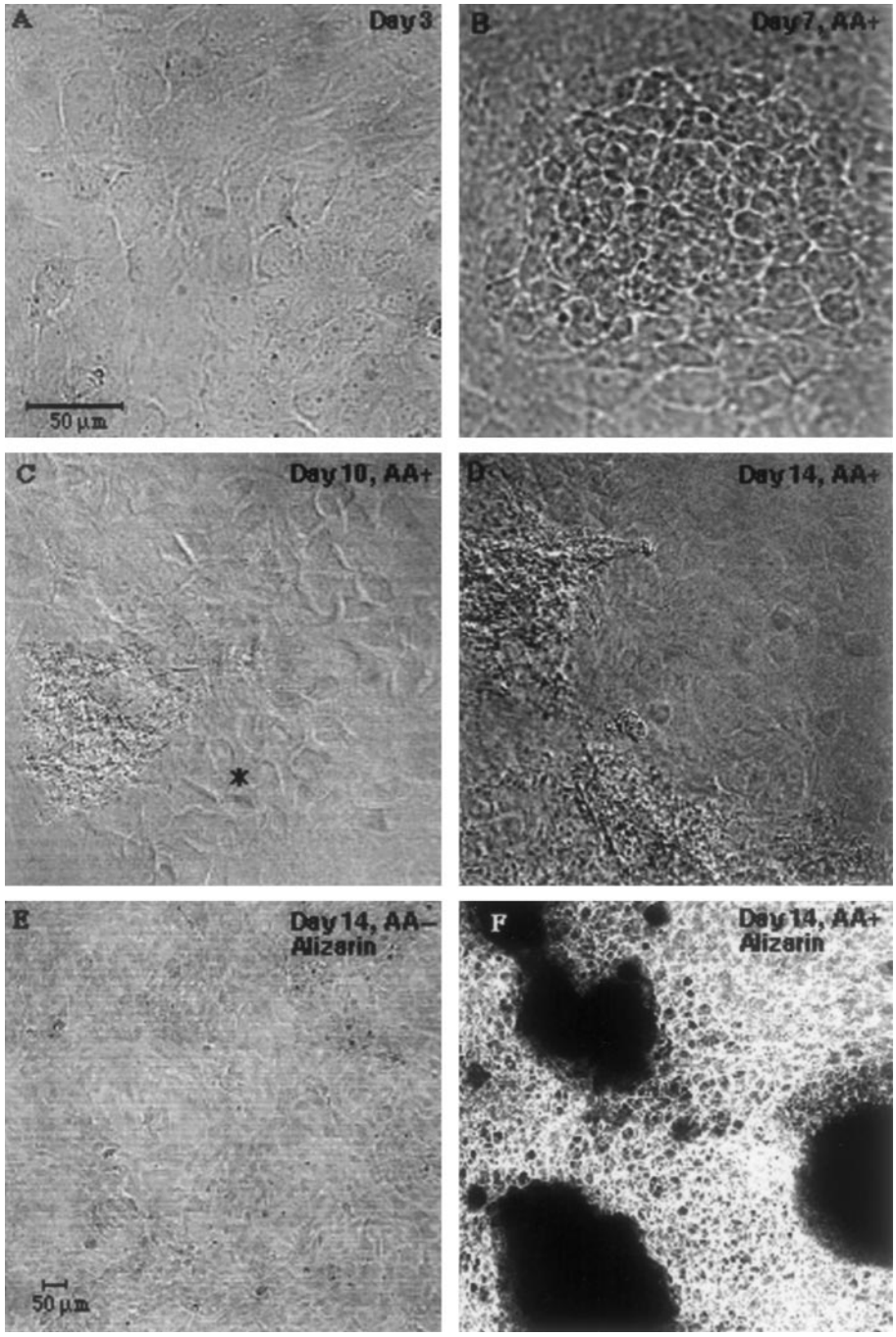

Fig. 1. Fetal rat calvarial osteoblasts differentiate to form bonelike mineralized nodules in culture. Cell were grown to confluence (*day 3*; *A*), and the medium was then supplemented with ascorbic acid (AA) and β-glycerophosphate (βGP) to induce differentiation. By *day 7* (*B*), discrete regions of cuboidal cells (nodules) first appeared in AA-treated cultures. By *day 10* (*C*), cells produced abundant extracellular matrix in AA-treated cultures. By *day 14* (*D*), nodules appeared phase dense. On *day 14*, cultures grown in AA-untreated (*E*) or AA-treated (*F*) medium were stained for mineralized matrix with alizarin red. *Example of site selected for imaging of mitochondria (detected by JC-1 staining) in nodule cells shown in Fig. 4. Bar = 50 μm.

extracellular matrix (26), demonstrated a low level of autofluorescence that obscured the fluorescent signal generated by JC-1 (data not shown). Therefore, we selected for analysis specific sites within nodules in which the cells display a distinctive cuboidal morphology characteristic of mature osteoblasts (a representative site is marked with an asterisk on Fig. 1*C*). AA-untreated cultures demonstrated predominantly low-$\Delta\psi$ mitochondria, with few high-$\Delta\psi$ mitochondria on *day 10* (Fig. 4, *A–C*). In contrast, nodule cells in AA-treated cultures possessed abundant high-$\Delta\psi$ mitochondria (Fig. 4, *D–F*). To quantitate these differences in numbers of high- and low-$\Delta\psi$ mitochondria, the ratio of the number of pixels in each channel throughout the entire image stack was determined. The ratio of red signal (high-$\Delta\psi$ mitochondria) to green signal (low-$\Delta\psi$ mitochondria) was 0.1 in AA-untreated cells, whereas the ratio was 0.6 in AA-treated cells.

As a control, mature cultures were treated with FCCP, a proton ionophore that abolishes the mitochondrial electrochemical gradient. Addition of the inhibitor eliminated the appearance of red fluorescence in AA-treated osteoblasts (Fig. 4, *G–I*). The green fluorescence was retained in FCCP-treated cultures (although the mitochondria appeared swollen), indicating that cells were capable of sequestering the dye despite

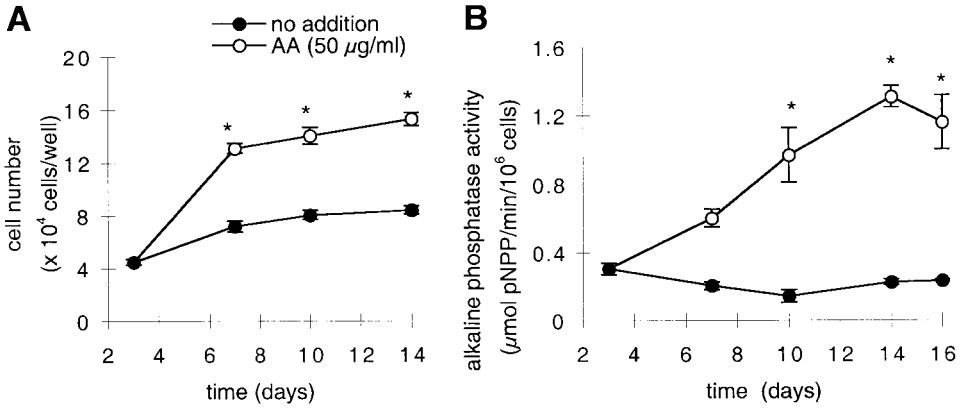

Fig. 2. Osteoblast differentiation increases cell number and alkaline phosphatase activity. Osteoblasts were grown to confluence (*day 3*). On *day 3*, medium was supplemented (○) or not (●) with AA and βGP, and samples were recovered at the indicated times to measure cell number (*A*) and alkaline phosphatase activity (*B*). *Significantly different compared with AA-untreated controls ($P < 0.05$).

treatment with inhibitor. Thus the fluorescent signal in the red channel detected with JC-1 reveals the location of high-Δψ mitochondria.

To assess the subcellular distribution of mitochondria, images of AA-treated cells stained with JC-1 were collected from the culture medium-facing surface, through the cell layer, to the surface adjacent to the plastic substrate of the dish (Fig. 5). The high-Δψ mitochondria in nodule cells were concentrated near the culture medium-facing surface, whereas low-Δψ mitochondria were distributed throughout the cell layers. Quantification of the fluorescence revealed that the ratio of pixels in the red channel (high-Δψ mitochondria) to those in the green channel (low-Δψ mitochondria) within the first 3 μm of the cell culture-facing surface of the cells was 0.8, whereas the ratio within 3 μm of the opposite surface was only 0.2. To confirm that the differences in red and green fluorescence observed at various positions in the nodules did not arise due to differential light penetration or photobleaching, we grew cells on coverslips and acquired the stack of images in reverse order (i.e., from the surface of the dish to the surface adjacent to the culture medium). The same results were obtained (not shown), confirming that high-Δψ mitochondria were concentrated near the culture medium-facing surface of the cells.

In addition, AA treatment appeared to affect the shape of mitochondria. Mitochondria in AA-untreated cells appeared longer and thinner than those in nodule cells. However, this can be attributed in large part to differences in the orientation of the organelles due to cell morphology, since maturing osteoblasts were cuboidal, whereas immature cells were well spread and flat (Fig. 1).

Cellular ATP content. Because respiration and mitochondrial activity changed markedly during differentiation, we measured cellular ATP content, which is normally maintained within narrow limits. In AA-untreated cells, the ATP levels in osteoblasts declined between *day 3* and *day 7* and then remained constant through the remaining 14-day period (Fig. 6). Surprisingly, treatment with AA caused ATP content per cell to rise threefold between *day 7* and *day 10*. On *day 14*,

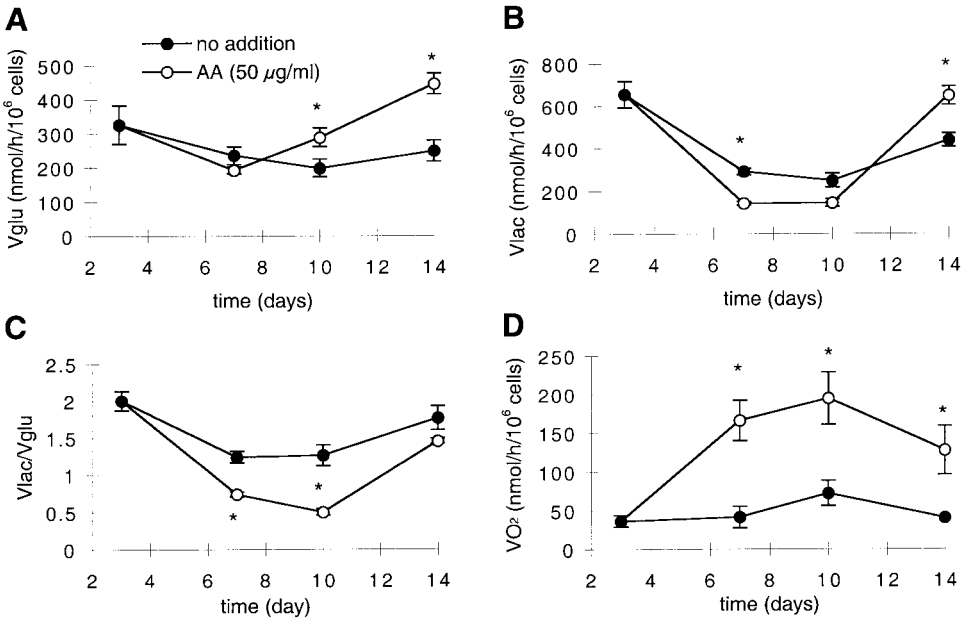

Fig. 3. Osteoblast differentiation coincides with changes in energy metabolism. Osteoblasts were grown to confluence (*day 3*). Medium was then supplemented (○) or not (●) with AA and βGP, and samples were recovered at the indicated times to measure the rate of glucose consumption ($\dot{V}_{glu}$; *A*), rate of lactate production ($\dot{V}_{lac}$; *B*), the ratio of $\dot{V}_{lac}$ to $\dot{V}_{glu}$ (*C*), and the rate of O_2 consumption ($\dot{V}O_2$; *D*). *Significantly different from AA-untreated controls ($P < 0.05$).

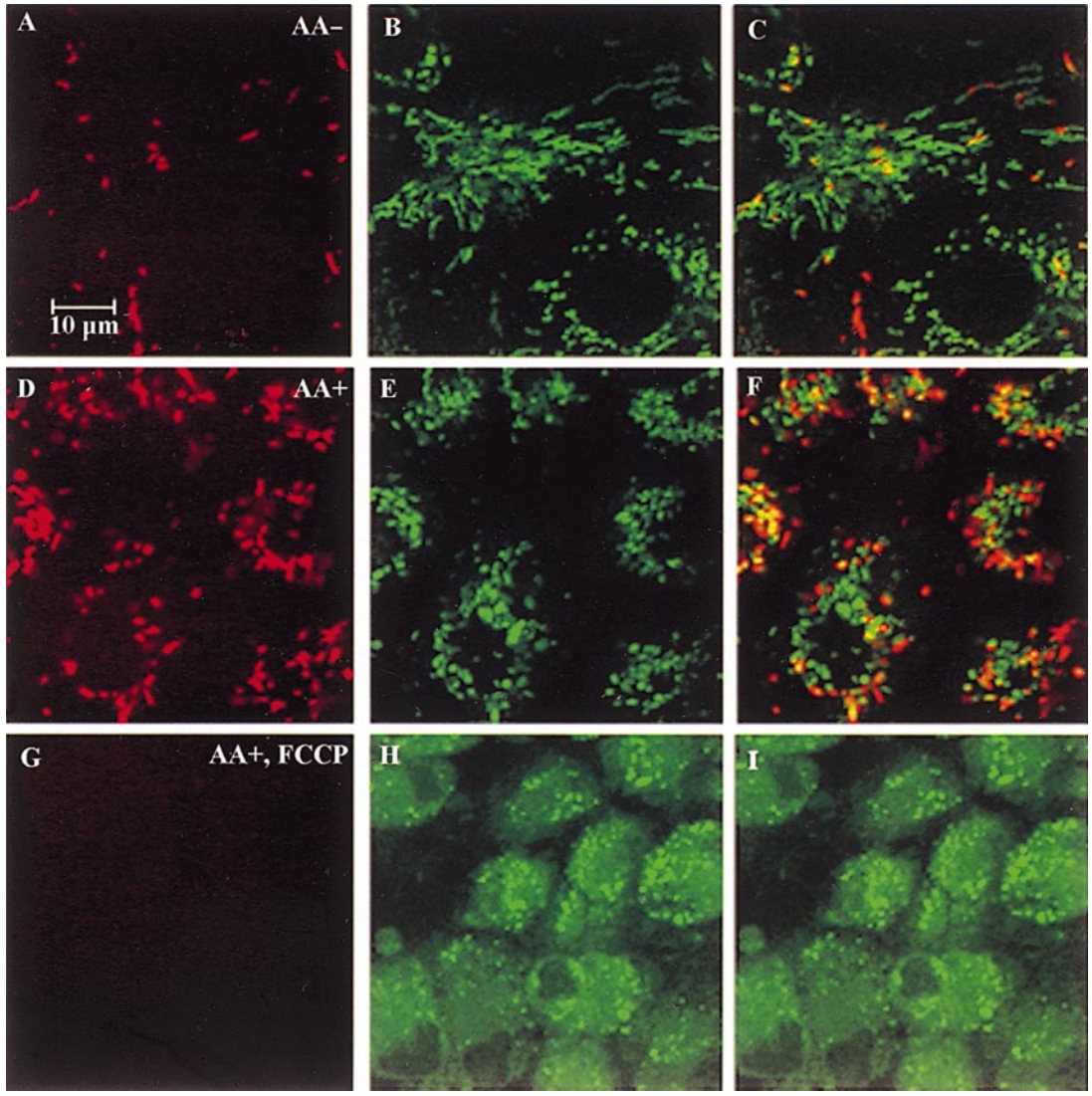

Fig. 4. Osteoblasts in nodules possess abundant high-transmembrane-potential ($\Delta\psi$) mitochondria. Osteoblasts were grown for 10 days in AA-untreated (*A–C*) or AA-treated (*E–I*) medium. AA-treated cultures were treated with FCCP to depolarize the mitochondria (*G–I*), demonstrating specificity of the signal. Cells were then incubated for 30 min with JC-1, a mitochondrial $\Delta\psi$-sensitive vital dye, and images were then collected by confocal microscopy. Single images ~4 μm from the cell culture-medium facing surface of the cells are shown. A representative site selected for analysis of mitochondrial $\Delta\psi$ in nodule cells is marked with an asterisk in Fig. 1. Red fluorescent images of dye aggregates indicate high-$\Delta\psi$ mitochondria (*A*, *D*, and *G*). Green fluorescent image of monomeric dye show low-$\Delta\psi$ mitochondria (*C*, *E*, and *H*). Composite images (*C*, *F*, and *I*) are also shown. Bar = 10 μm.

ATP levels in AA-treated cells were fivefold higher than in AA-untreated cells. To determine if the rise in cellular ATP content of AA-treated cells could be attributed to differences in volume, cell size was estimated by flow cytometry (Fig. 7). Osteoblasts grown for 10 days were dispersed and stained with PI and Hoechst dye to assess cell viability and then analyzed by flow cytometry. Forward light scatter by the cells provides an estimate of cell size and, hence, cell volume. The distribution of sizes in the viable cell population was found to be similar in AA-treated and AA-untreated cultures (Fig. 6). Therefore, the increase in total ATP per cell in AA-treated cells is unlikely to be caused by increased cells volume; rather, it reflects a higher concentration of ATP in individual cells.

Contribution of glycolysis vs. oxidative phosphorylation to ATP content in mature osteoblasts. To evaluate the contribution of glycolysis and respiration to maintaining the high ATP content of mature osteoblasts, metabolic inhibitors were added to AA-treated cells on *day 14* for 2–4 h. The addition of NaF, which inhibits glycolysis (13), caused a dose-dependent decrease in $\dot{V}_{glu}$ and $\dot{V}_{lac}$, effectively depleting cellular ATP content, whereas $\dot{V}O_2$ did not change significantly (Fig. 8). In contrast, the addition of an inhibitor of cytochrome *c* oxidase, NaN_3, caused a decrease in $\dot{V}O_2$ and an increase in the ratio of $\dot{V}_{lac}$ to $\dot{V}_{glu}$ to two at all concentrations of NaN_3 tested, showing that respiration was effectively abolished. Under these conditions, NaN_3 caused a 2-fold increase in $\dot{V}_{glu}$ and a 2.5-fold

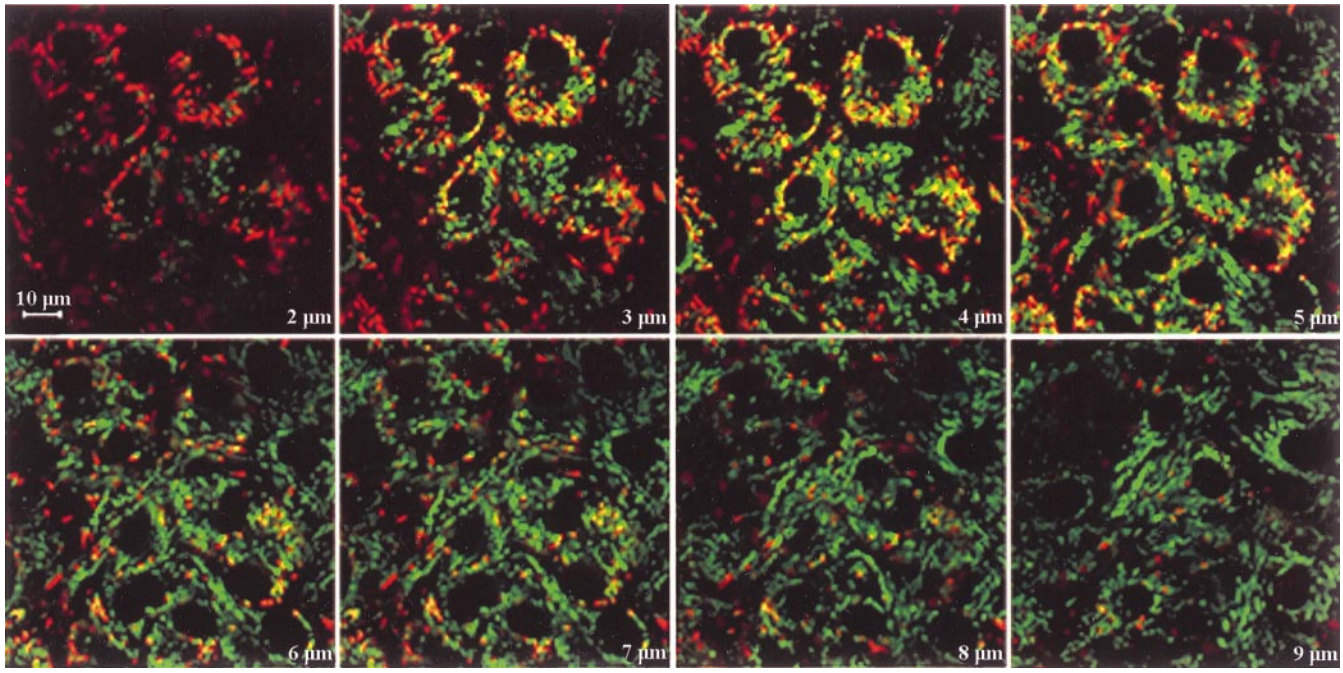

Fig. 5. High-Δψ mitochondria are concentrated near the culture medium-facing surface of mature osteoblasts. Cells were grown for 10 days in AA-treated medium and then incubated for 30 min with JC-1. Three-dimensional image stacks were collected by scanning confocal microscopy. Composite images show high-Δψ mitochondria (red) and low-Δψ mitochondria (green) at increasing distances (in μm) from the cell surface facing the culture medium (top of the nodule) to the surface adjacent to the dish (bottom of the nodule). Bar = 10 μm.

increase in $\dot{V}_{lac}$. Notably, the cellular levels of ATP were not significantly affected after 4 h of incubation with NaN_3. Similar results were obtained with KCN, another inhibitor of cytochrome *c* oxidase. Thus, in mature osteoblasts, ATP levels were maintained by an apparent increase in $\dot{V}_{glu}$ and $\dot{V}_{lac}$, despite complete inhibition of mitochondrial respiration.

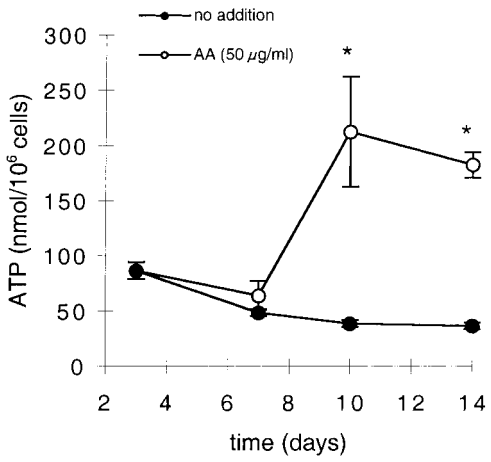

Fig. 6. Osteoblast differentiation coincides with an increase in cellular ATP content. Osteoblasts were grown to confluence (*day 3*); medium was then supplemented (○) or not (●) with AA and βGP. Cells were then harvested for measurements of total cellular ATP and cell number, and results are expressed as nmol ATP/10^6 cells. *Significantly different compared with AA-untreated controls ($P < 0.05$).

DISCUSSION

Results from this study revealed that the progression of cultured osteoblasts through sequential stages of differentiation coincided with marked changes in metabolic and mitochondrial activity. The sequence of major changes evident during differentiation were as follows: first, the rate of respiration increased during active growth of the cells to form multilayers and initiate differentiation (*days 3–7*); second, the ATP content of maturing cultures increased during nodule morphogenesis (*days 7–10*); and, third, the rate of glycolysis rose during nodule mineralization (*days 10–14*). Mature cells also demonstrated increased numbers of high-Δψ mitochondria relative to immature cells. Thus both glycolytic and mitochondrial changes appear to be integral components of the differentiation sequence in cultured osteoblasts.

During the first stage of differentiation that we studied (*days 3–7*), the rate of cellular respiration in maturing osteoblasts rose markedly. During this period, the addition of AA caused a doubling in cell number and the formation of multilayers, alkaline phosphatase activity rose sevenfold, and morphologically distinct nodules first appeared. These changes coincided with a 3-fold increase in $\dot{V}O_2$, a 2-fold decrease in $\dot{V}_{lac}$, and a 1.4-fold decrease in the ratio of $\dot{V}_{lac}$ to $\dot{V}_{glu}$. Together, these results suggest that, by *day 7*, more of the pyruvate produced by glycolysis was consumed in the Krebs cycle in mature osteoblasts compared with immature cells, and oxidative phosphorylation increased. Cells

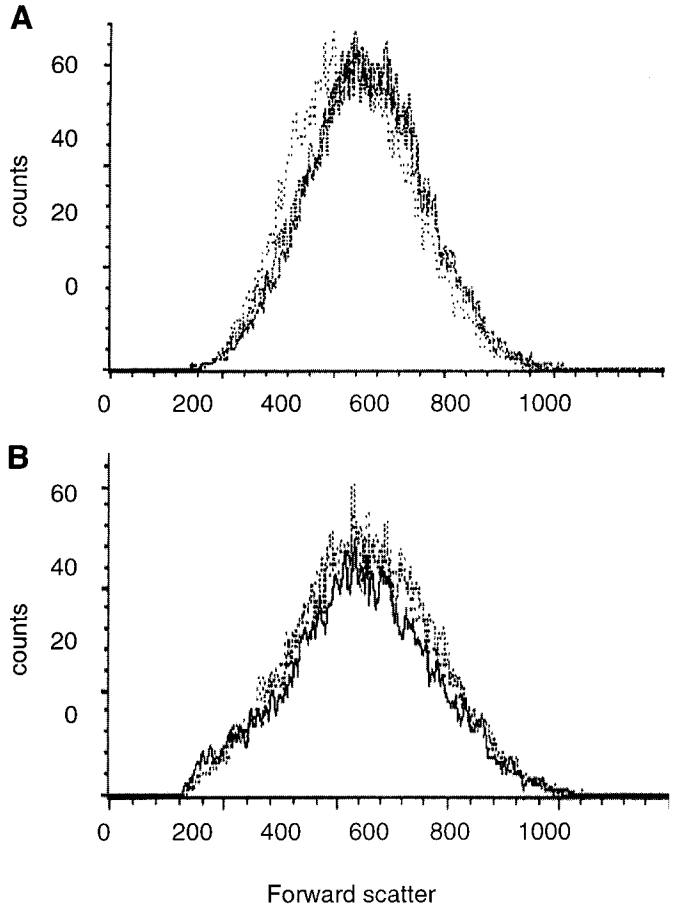

Fig. 7. Cell sizes of viable osteoblasts from AA-treated and AA-untreated cultures are comparable, as estimated by flow cytometry. Osteoblasts were grown to confluence (*day 3*) and then were grown without (*A*) or with (*B*) the addition of AA. Samples were recovered on *day 10*, dispersed, stained with propidium iodide and Hoechst dye to identify viable cells, and then analyzed by flow cytometry. Histograms of forward light scatter for viable cells from 3 separate cell samples for each group are shown.

that were grown without AA failed to differentiate and did not increase in $\dot{V}O_2$, whereas $\dot{V}_{lac}$ declined, although to a lesser extent than in maturing osteoblasts. Thus cellular aging, as well as differentiation, induced changes in glycolysis over time in cultured osteoblasts. The early and sustained rise in the respiratory rate of maturing osteoblasts is likely to reflect the high metabolic demands placed on cells when they are dividing and differentiating and is consistent with the finding that $\dot{V}O_2$ is high in intact bone tissue (30). Similarly, oxidative phosphorylation increases during differentiation of other cell types in vitro, including, for example, placental trophoblasts (3), nerve cells (6), and colon adenocarcinoma cells (10).

The most notable feature of the second stage of differentiation (*days 7–10*) was an increase in cellular ATP content. During this stage, cell growth slowed, alkaline phosphatase activity continued to rise, and nodules further matured as more extracellular matrix was produced. We showed previously that expression of protein for the late osteoblast marker, osteocalcin, is restricted to nodules on *day 8* and mRNA transcripts are detectable with the use of Northern blotting on *day 10* (11, 26); thus this period of culture corresponds to a stage of advancing maturation. These changes in differentiation were accompanied by an unexpected fivefold increase in ATP content, compared with cells grown without AA, when corrected on a per cell basis. Typically, cellular ATP content does not change markedly in response to nonpathological stimuli (e.g., Ref. 6). Differentiation of erythroid precursor cells leads to a decline in cellular ATP content (corrected for cell number), although this difference can be attributed to a reduction in cell volume as these cells mature such that the intracellular concentration of ATP remains constant (19).

To address the possibility that cytosolic volume increases during osteoblast differentiation, which could conceivably account for the observed rise in cellular ATP content, we examined in detail the distribution of cell sizes within cultured osteoblasts using a flow cytometry method that distinguishes viable cells from dead cells. Results from these experiments demonstrated that the size distributions of viable cells from AA-treated and untreated cultures were comparable, indicating that the intracellular concentration of ATP was in fact higher in mature osteoblasts than in immature cells.

The functional consequence(s) of the increased ATP pool size in maturating osteoblasts is unknown. One possibility is that adenylate metabolism regulates intracellular ATP and the total adenylate pool to control

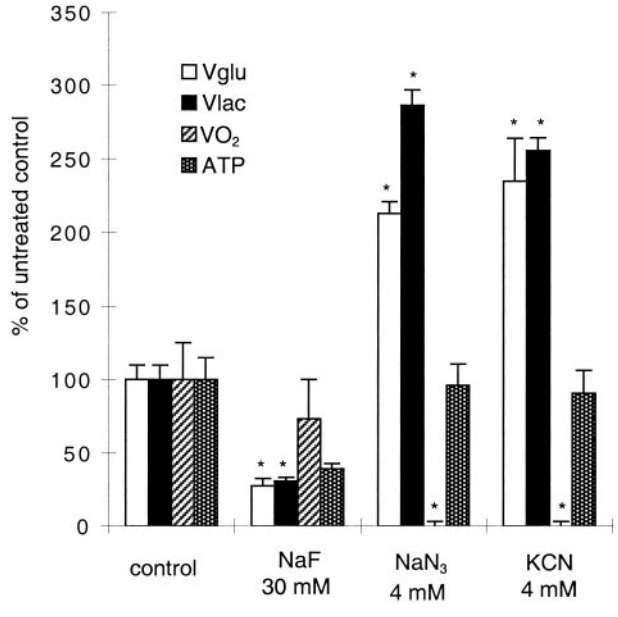

Fig. 8. Effects of inhibitors of glycolysis and oxidative phosphorylation on the energy metabolism of mature osteoblasts. Osteoblasts were grown to confluence (*day 3*); medium was then supplemented with AA and βGP. On *day 14*, NaF (30 mM), NaN_3 (4 mM), or potassium cyanide (KCN; 4 mM) was added to the incubation media as described in MATERIALS AND METHODS. Measurements of $\dot{V}_{glu}$, $\dot{V}_{lac}$, and $\dot{V}O_2$ were made over 4 h. ATP was measured after 4 h of treatment with inhibitor. *Significantly different compared with AA-untreated controls ($P < 0.05$).

ATP-dependent processes, such as the activity of ion pumps (1, 2). In addition, ATP produced by osteoblasts may function as a paracrine agonist. ATP binds to purinergic receptors on osteoblasts, stimulating calcium signaling (22) and affecting osteogenesis (18). Thus an enlarged pool of ATP may be stored in mature osteoblasts for later secretion in response to appropriate stimuli, such as mechanical forces (7).

Once differentiation progressed to the stage in which abundant extracellular matrix was evident in the nodules (*day 10*), a marked difference in mitochondrial activity was also observed. Three-dimensional confocal imaging using the mitochondrial $\Delta\psi$-sensitive dye JC-1 demonstrated that mature osteoblasts contained a larger number of high-$\Delta\psi$ mitochondria than immature osteoblasts. These results are consistent with studies of Klein et al. (20, 21) who showed that bone marrow stromal cell populations accumulate more rhodamine 123 dye when treated with medium that promotes the differentiation of osteoprogenitors.

High-$\Delta\psi$ mitochondria were preferentially distributed at the cell culture medium surface of nodule cells, whereas the low-$\Delta\psi$ mitochondria were more evenly distributed throughout the cell. On the basis of the preferential distribution of enveloped viral glycoproteins, the cell culture-facing surface of polarized osteoblasts corresponds to the basolateral surface of epithelial cells (17). The polar distribution of mitochondria in these primary cells contrasts with the results obtained using cell lines, in which mitochondria are localized to the edges of cells (5). The precise consequence of localized regions of high-$\Delta\psi$ mitochondria is not yet known, although Reers et al. (28) suggest that they are hot spots for ATP generation or calcium signaling; in contrast, the low-$\Delta\psi$ mitochondria may be metabolically less active. Treatment of immature osteoblasts in culture with PTH causes a modest decline in $\Delta\psi$ as shown by JC-1 staining (33); results obtained from this study indicate that the stage of cellular differentiation is likely to affect changes in mitochondrial $\Delta\psi$ responses to calciotropic stimuli.

The most notable metabolic feature of the final stage of differentiation (*days 10–14*) was an abrupt rise in $\dot{V}_{lac}$. During this stage, mineralization of nodules occurred and alkaline phosphatase peaked on *day 14*. Metabolically, $\dot{V}O_2$ and ATP content remained constant, whereas $\dot{V}_{glu}$ rose. Together with the increase in $\dot{V}_{lac}$, these results suggest that there is a marked increase in the rate of glycolysis at this latter stage of differentiation. The total rate of ATP production from glucose was estimated at 900 $nmol \cdot h^{-1} \cdot 10^6$ $cells^{-1}$ by glycolysis and 800 $nmol \cdot h^{-1} \cdot 10^6$ $cells^{-1}$ by oxidative phosphorylation. Thus glycolysis provided ~50% of the energy requirements of mature osteoblasts and is likely to be important for the function of mature cells. In fact, inhibition of oxidative phosphorylation using NaN_3 or KCN for 2–4 h led to a rapid increase in $\dot{V}_{lac}$ and $\dot{V}_{glu}$ by osteoblasts, and cellular ATP content was thereby maintained at high levels for at least 4 h. In contrast, acute inhibition of glycolysis using NaF did not affect $\dot{V}O_2$, and ATP levels declined sharply, indicating that respiration did not compensate for the loss of glycolytic activity. Interestingly, the maximum capacity of the respiratory inhibitors to stimulate glycolytic activity in mature cells was of the same magnitude (2- to 2.5-fold) as that which occurs when bone tissue is exposed to hypoxic conditions in vitro (4). Thus the glycolytic component of energy generation at this mature stage of osteoblast differentiation may play a key role in adapting to transient challenges such as changes in either O_2 supply to bone or increases in the acute and transient demands for energy.

We thank Eduardo Almeida at the University of California, San Francisco, and Paul Dazin at the Howard Hughes Medical Center at the University of California, San Francisco, for help with the flow cytometry analyses. We also thank Nancy Searby and Sigrid Reinsch for helpful advice during the study and Charles Wade and Sigrid Reinsch for critical reading of the manuscript.

This work was supported by NASA Grant NAGS5-6374, a DDF award for the Core Confocal Microscopy facility at Ames Research Center, and a National Research Council Postdoctoral Fellowship (to S. V. Komarova).

Current address of S. V. Komarova: Dept. of Physiology, University of Western Ontario, London, Ontario, Canada.

REFERENCES

1. **Aprille J.** Regulation of the mitochondrial adenine nucleotide pool size in liver: mechanism and metabolic role. *FASEB J* 2: 2547–2556, 1988.
2. **Ataullakhanov F, Martynov M, Komarova S, and Vitvitsky V.** A possible role of adenylate metabolism in human erythrocytes. 2. Adenylate metabolism is able to improve the erythrocyte volume stabilization. *J Theor Biol* 183: 307–316, 1996.
3. **Bax B and Bloxam D.** Energy metabolism and glycolysis in human placental trophoblast cells during differentiation. *Biochim Biophys Acta* 283: 283–292, 1997.
4. **Borle A, Nichols N, and Nichols G.** Metabolic studies of bone in vitro. I. Normal bone. *J Biol Chem* 235: 1211–1214, 1960.
5. **Diaz G, Setzu M, Zucca A, Isola R, Diana A, Murru R, Sogos V, and Gremo F.** Subcellular heterogeneity of mitochondrial membrane potential: relationship with organelle distribution and intercellular contacts in normal, hypoxic and apoptotic cells. *J Cell Sci* 112: 1077–1084, 1999.
6. **Dittmann L, Hertz L, Schousboe A, Fosmark H, Sensenbrenner M, and Mandel P.** Energy metabolism of nerve cells during differentiation. *Exp Cell Res* 80: 425–431, 1973.
7. **Dixon S, Kaplan A, Naemsch L, Sims S, Underhill T, and Weidema A.** P2 purinoceptors in skeletal cells: receptor subtypes, signalling pathways, and possible role in mechanotransduction. In: *Biological Mechanisms of Tooth Eruption, Resorption and Replacement by Implants,* edited by Davidovitch Z and Mah J. Boston, MA: Harvard Society for the Advancement of Orthodontics, 1998, p. 301–314.
8. **Dodd J, Raleigh J, and Gross T.** Osteocyte hypoxia: a novel mechanotransduction pathway. *Am J Physiol Cell Physiol* 277: C598–C602, 1999.
9. **Felix R, Neuman W, and Fleisch H.** Aerobic glycolysis in bone: lactic acid production by rat calvaria cells in culture. *Am J Physiol Cell Physiol* 234: C51–C55, 1978.
10. **Galons JP, Fantini J, Vion-Dury J, Cozzone P, and Canioni P.** Metabolic changes in undifferentiated and differentiated human colon adenocarcinoma cells studied by multinuclear magnetic resonance spectroscopy. *Biochimie* 71: 949–961, 1989.
11. **Globus R, Doty S, Lull J, Holmuhamedov E, Humphries M, and Damsky C.** Fibronectin is a survival factor for differentiated osteoblasts. *J Cell Sci* 111: 1385–1393, 1998.
12. **Green D and Reed J.** Mitochondria and apoptosis. *Science* 281: 1309–1312, 1998.
13. **Guidicelli Y, Pecquery R, Provin D, Agli B, and Nordmann R.** Regulation of lipolysis and cyclic AMP synthesis through

energy supply in isolated human fat cells. *Biochim Biophys Acta* 23: 385–398, 1977.
14. **Hamel W, Dazin P, and Israel M.** Adaptation of a simple flow cytometric assay to identify different stages during apoptosis. *Cytometry* 25: 173–181, 1996.
15. **Ichas F, Jouaville L, and Mazat J.** Mitochondria are excitable organelles capable of generating and conveying electrical and calcium signals. *Cell* 89: 1145–1153, 1997.
16. **Ilic D, Almeida E, Schlaepfer D, Dazit P, Aizawa S, and Damsky C.** Extracellular matrix survival signals transduced by focal adhesion kinase suppress p53-mediated apoptosis. *J Cell Biol* 143: 547–560, 1998.
17. **Ilvesaro J, Metsikko K, Vaananen K, and Tuukkanen J.** Polarity of osteoblasts and osteoblast-like UMR-108 cells. *J Bone Miner Res* 14: 1339–1344, 1999.
18. **Jones S, Gray C, Boyde A, and Burnstock G.** Purinergic transmitters inhibit bone formation by cultured osteoblasts. *Bone* 21: 393–399, 1997.
19. **Kim H, Koury M, Lee S, Im J, and Sawyer S.** Metabolic adaptation during erythropoietin-mediated terminal differentiation of mouse erythroid cells. *Blood* 77: 387–392, 1991.
20. **Klein B, Gal I, Hartshtark Z, and Segal D.** Induction of osteoprogenitor cell differentiation in rat marrow stroma increases mitochondrial retention of rhodamine 123 in stromal cells. *J Cell Biochem* 53: 190–197, 1993.
21. **Klein B, Gal I, Libergal M, and Ben-Bassat H.** Opposing effects on mitochondrial membrane potential by malonate and levamisole, whole effect on cell-mediated mineralization is antagonistic. *J Cell Biochem* 60: 139–147, 1996.
22. **Kumegai H, Sakamoto H, Guggino S, Filburn C, and Saktor B.** Purinergic regulation of cytosolic calcium in osteoblast-like bone cells. *Calcif Tissue Int* 45: 251–254, 1989.
23. **Lynch M, Capparelli C, Stein J, Stein G, and Lian J.** Apoptosis during bone-like tissue development in vitro. *J Cell Biochem* 68: 31–49, 1998.
24. **Malaval L, Modrowski D, Gupta AK, and Aubin JE.** Cellular expression of bone-related proteins during in vitro osteogenesis in rat bone marrow stromal cell cultures. *J Cell Physiol* 158: 555–572, 1994.
25. **Mancini M, Anderson B, Caldwell E, Seghinasab M, Paty P, and Hockenbery D.** Mitochondrial proliferation and paradoxical membrane depolarization during terminal differentiation and apoptosis in a human colon carcinoma cell line. *J Cell Biol* 138: 449–469, 1997.
26. **Moursi A, Damsky C, Lull J, Zimmerman D, Doty S, Aota S, and Globus R.** Fibronectin regulates calvarial osteoblast differentiation. *J Cell Sci* 109: 1369–1380, 1996.
27. **Owen TA, Aronow M, Shalhoub V, Barone LM, Wilming L, Tassinari MS, Kennedy MB, Pockwinse S, Lian JB, and Stein GS.** Progressive development of the rat osteoblast phenotype in vitro: reciprocal relationships in expression of genes associated with osteoblast proliferation and differentiation during formation of the bone extracellular matrix. *J Cell Physiol* 143: 420–430, 1990.
28. **Reers M, Smiley S, Mottola-Hartshorn C, Chen A, Lin M, and Chen L.** Mitochondrial membrane potential monitored by JC-1 dye. *Methods Enzymol* 260: 403–417, 1995.
29. **Salvioli S, Ardizzoni A, Franceschi C, and Cossarizza A.** JC-1, but not DiOC6(3) or rhodamine123, is a reliable fluorescent probe to assess mitochondrial transmembrane potential changes in intact cells: implications for studies on mitochondrial functionality during apoptosis. *FEBS Lett* 411: 77–82, 1997.
30. **Schirrmacher K, Lauterbach S, and Bingmann D.** Oxygen consumption of calvarial bone cells in vitro. *J Orthop Res* 15: 558–562, 1997.
31. **Shapiro I and Haselgrove J.** Energy metabolism in bone. In: *Bone,* edited by Hall B. Boca Raton, FL: CRC, 1992, p. 99–140.
32. **Somjen D, Weisman J, Harell A, Burger E, and Kaye A.** Direct and sex-specific stimulation by sex steroids of creatine kinase activity and DNA synthesis in rat bone. *Proc Natl Acad Sci USA* 86: 3361–3365, 1989.
33. **Troyan M, Gilman V, and Gay C.** Mitochondrial membrane potential changes in osteoblasts treated with parathyroid hormone and estradiol. *Exp Cell Res* 233: 274–280, 1997.